Advances in Water Resources 50 (2012) 152–161

Contents lists available at SciVerse ScienceDirect

Advances in Water Resources

journal homepage: www.elsevier.com/locate/advwatres

Soil water content estimation using a remote sensing based hybrid evapotranspiration modeling approach ☆

Christopher M.U. Neale [a,*], Hatim M.E. Geli [a], William P. Kustas [b], Joseph G. Alfieri [b], Prasanna H. Gowda [c], Steven R. Evett [c], John H. Prueger [d], Lawrence E. Hipps [e], Wayne P. Dulaney [b], José L. Chávez [f], Andrew N. French [g], Terry A. Howell [c]

[a] Civil and Environmental Engr., Utah State Univ., 4110 Old Main Hill, Logan, UT 84322-4110, United States
[b] USDA-Agricultural Research Service, Hydrology & Remote Sensing Laboratory, Bldg. 007, BARC-West, Beltsville, MD 20705, United States
[c] USDA-ARS Conservation and Production Research Laboratory, P.O. Drawer 10, Bushland, TX 79012, United States
[d] USDA-ARS National Lab for Agriculture and the Environment, 2110 Univ. Blvd., Ames, IA 50011, United States
[e] Plants, Soils & Climate Depart., Utah State Univ., 4820 Old Main Hill, Logan, UT 84322-4820, United States
[f] Dept. of Civil & Environ. Engr., Colorado State Univ., 1372 Campus Deliv., Fort Collins, CO 80523, United States
[g] USDA-ARS Arid-Land Agricultural Research Center, 21881 North Cardon Lane, Maricopa, AZ 85238, United States

ARTICLE INFO

Article history:
Available online 2 November 2012

Keywords:
Airborne remote sensing
Evapotranspiration
Soil water content
Energy balance
Crop coefficients

ABSTRACT

Remote sensing of evapotranspiration (ET) has evolved over the last 20 years with the development of more robust energy balance approaches and the availability of timely remotely sensed imagery from satellite sensors. This has allowed the use of remote sensing for near-real time water management in irrigated systems in the western United States. In this paper a hybrid ET approach is applied to irrigated and non-irrigated cotton fields at the BEAREX08 experimental site using airborne remote sensing inputs under highly advective conditions, taking advantage of the available root zone soil water content measurements for verification of model output. The modeling approach is based on coupling the Two-Source-Energy Balance (TSEB) and the reflectance-based crop coefficient models. The TSEB model provides estimates of real crop ET while the reflectance-based crop coefficient approach allows for updating the basal crop coefficient and the interpolation and extrapolation of ET between the dates of remote sensing inputs facilitating the maintenance of a soil water balance in the root zone of the crop. Actual ET estimates using the TSEB model were compared with measured ET using eddy covariance systems deployed in four cotton fields during the BEAREX08 experiment. Estimates of soil water content in the soil profile of both irrigated and rain fed cotton fields were compared with measurements at different depths using neutron probe observations. Data assimilation techniques were applied to update soil water content values using estimates based on actual ET from the TSEB model. Results indicate that the hybrid ET modeling approach using data assimilation produced reliable daily ET interpolated between remote sensing observations and significantly improved soil water content estimates throughout the root zone profile compared to applying the crop-coefficient technique in a water balance model without the actual ET inputs.
© 2012 Elsevier Ltd. All rights reserved.

1. Introduction

Remote sensing approaches for routine estimation of evapotranspiration (ET) over large regions are becoming more readily available [1–3]. These models are based on the solution of the energy balance equation, using shortwave and longwave band inputs from satellite sensors to estimate net radiation (*Rn*), soil heat flux (*G*) and sensible heat flux (*H*) with the latent heat flux (*LE*) obtained as a residual ($LE = Rn - G - H$). The *LE* can then be extrapolated from a quasi-instantaneous value at the time of the satellite overpass to a daily ET value using different methods such as the evaporative fraction or the reference ET fraction [4,5]. Energy balance methods vary in complexity mainly in the way they parameterize and solve for *H*. The main advantage of thermal-based

☆ The U.S. Department of Agriculture (USDA) prohibits discrimination in all its programs and activities on the basis of race, color, national origin, age, disability, and where applicable, sex, marital status, familial status, parental status, religion, sexual orientation, genetic information, political beliefs, reprisal, or because all or part of an individual's income is derived from any public assistance program. (Not all prohibited bases apply to all programs.) Persons with disabilities who require alternative means for communication of program information (Braille, large print, audiotape, etc.) should contact USDA's TARGET Center at (202) 720-2600 (voice and TDD). To file a complaint of discrimination, write to USDA, Director, Office of Civil Rights, 1400 Independence Avenue, S.W., Washington, DC 20250-9410, USA or call +1 (800) 795 3272 (voice) or +1 (202) 720 6382 (TDD). USDA is an equal opportunity provider and employer.

* Corresponding author. Tel.: +1 4357973689; fax: +1 4357971185.
E-mail address: christopher.neale@usu.edu (C.M.U. Neale).

0309-1708/$ - see front matter © 2012 Elsevier Ltd. All rights reserved.
http://dx.doi.org/10.1016/j.advwatres.2012.10.008

energy balance models is that by solving for H, these models relate actual ET and soil water state to the surface-air temperature difference, requiring no soil profile information.

Single-source models such as the Soil Energy Balance for Land (SEBAL; 2) and the Mapping EvapoTranspiration at high Resolution with Internalized Calibration (METRIC; 3), solve for H through a relationship with dT, the near-surface air temperature gradient obtained by solving the energy balance over carefully selected "hot and cold" (or dry and wet) pixels identified using the thermal (radiometric surface temperature) and shortwave (surface albedo and the normalized difference vegetation index, NDVI) bands of the satellite image. An advancement to the original dT formulation of Bastiaansen et al. [2], was proposed by Allen et al. [3], where dT represents a temperature gradient elevated well above the surface that is linearly related to surface temperature adjusted to a common elevation for each image. This process bounds the energy balance within an irrigated area to these two extreme conditions, circumventing the need for estimating the "elusive" surface aerodynamic temperature in the bulk aerodynamic formulation of H which could vary according to surface type, soil water content, atmospheric stability and vegetation density.

The Two-Source-Energy-Balance (TSEB) model proposed by Norman et al. [6] computes components of Rn, H and LE fluxes separately for soil surface and canopy elements. The fraction of canopy cover obtained from shortwave band remote sensing is used to modulate the contributions from soil and canopy within the coarser thermal infrared pixel. This model has shown versatility in its application to both semi-arid environments with water-limited natural vegetation as well as in irrigated areas where soil water content is not limited [7]. The TSEB model requires calibrated thermal-infrared observations adjusted for atmospheric effects and corrected for surface emissivity in the thermal infrared band to produce accurate results.

Another remote sensing method used to estimate ET in irrigated areas is the reflectance-based crop coefficient approach, K_{cbrf} [8,9] where spectral inputs in the red and near-infrared bands are used to obtain a vegetation index such as the NDVI [10] or the Soil Adjusted Vegetation Index (SAVI) [11] which in turn is related to the basal crop coefficient, K_{cb} [12,13] through a simple linear transformation. In this approach, a time series of satellite image inputs tracks the crop growth in each field throughout the growing season with vegetation indices that are used to obtain the real-time K_{cbrf} and adjust the K_{cb} to match the actual growth conditions. The K_{cb}, by definition yields the potential crop ET for a certain leaf area under a dry soil surface condition (minimum evaporation) and no limitation of soil water content in the root zone (potential transpiration). In order to obtain the actual ET using the K_{cb}, a running soil water balance calculation must be maintained for the root zone, so that decreases in transpiration due to soil water deficit or increases in soil evaporation due to an irrigation or rain can be used to adjust the K_{cb} into the crop coefficient (K_c) [$K_c = K_s \times K_{cb} + K_e$, where K_s is the soil water deficit coefficient (0–1) and K_e is an adjustment to K_{cb} for wet soil surface conditions from rainfall or irrigation].

The crop coefficient approach is a simple empirical method that has been used with success over the past 30 years for irrigation planning as well as for irrigation scheduling of individual fields and estimates of ET over large irrigated areas. The use of spectral inputs to track the basal crop coefficient takes into account the actual crop growth and its in-field variability due to soil texture and variations in water content, non-uniform irrigation and fertilizer applications and other environmental factors. One of the main advantages of using basal crop coefficients is that they provide a modeling framework for interpolating and estimating daily ET of an irrigated area between intermittent satellite coverage. This allows monitoring ET during critical crop physiological stages during the growing season when there may be missing remotely-sensed imagery due to cloud cover. Such gaps in remote sensing information could reach a month or more when using Landsat Thematic Mapper which has a 16-day revisit time. Missing images can be particularly problematic during the active growth stage of many crops, where there is a rapid increase in vegetation biomass. The crop coefficient approach requires reliable weather station data collected within the area being modeled in order to estimate the reference evapotranspiration and calculate a soil water balance on a daily basis. This requires information on soil texture properties related to the water holding capacity.

Clearly there are advantages and disadvantages to both the thermal-based and crop-coefficient based techniques for ET estimation. An attempt in leveraging the strengths of both approaches and developing a "hybrid" remote sensing approach for estimating ET originally proposed by Neale et al. [14] has been developed into a fully operational modeling systems by Geli [15]. This approach consists of combining a thermal-based energy balance model for estimating the actual ET of the crop and the reflectance-based crop coefficient method to update the basal crop coefficient, tracking the growth of the crop and allowing for the interpolation of ET estimates in between remote sensing observation dates. The objective of this research is to rigorously evaluate the "hybrid" remote sensing approach for estimating ET, using data collected during the Bushland Evapotranspiration and Agricultural Remote sensing Experiment 2008 (BEAREX08) experiment [16]. This allowed for a detailed evaluation of the capability of this modeling approach in estimating ET and soil profile water content in a highly advective rainfed and irrigated crop environment. Measurements included high resolution airborne remotely sensed images, ET estimates using eddy covariance flux towers and profile soil water content measurements to a depth below 1 meter. Such an extensive set of measurements to thoroughly test model output were not available in a previous model validation study, nor was the model applied under such strongly advective conditions [15], which poses a significant challenge for remote sensing-based ET models that attempt to extrapolate instantaneous estimates obtained from imagery typically acquired in the morning hours, prior to cloud development, to daily values which are subject to strong advective conditions that usually occurs or intensifies in the afternoon hours.

2. Data

2.1. Research site

The data were collected in two dry land and two irrigated cotton fields located at the USDA-ARS, Conservation and Production Research Laboratory (CPRL), in Bushland, TX (35°11′N, 102°06′W). The elevation is approximately 1170 m above mean sea level. Each field was approximately 4.7-ha square in size, planted to cotton (*Gossypium hirsutum*). The soils in the experimental fields are classified as Pullman clay loam. Eddy covariance (EC) surface energy balance/flux towers were installed in the northeast corner of each field to maximize the upwind fetch in the predominant wind direction from the southwest (Fig. 1). These systems measured turbulent fluxes (H and LE) as well as the net radiation (Rn) and soil heat flux (G). A detailed description of the instrumentation and post processing of the EC data is presented in Alfieri et al. [17]. Meteorological data such as air temperature, wind speed, vapor and atmospheric pressure were obtained from the EC towers at nominally 2–2.5 m above ground level (agl). In addition, an automated weather station located within a small grass field east of the cotton fields provided meteorological data throughout the year on an hourly or 15-min basis which was used to estimate the reference evapotranspiration using the Penman-Monteith equation [13] and provide precipitation for updating

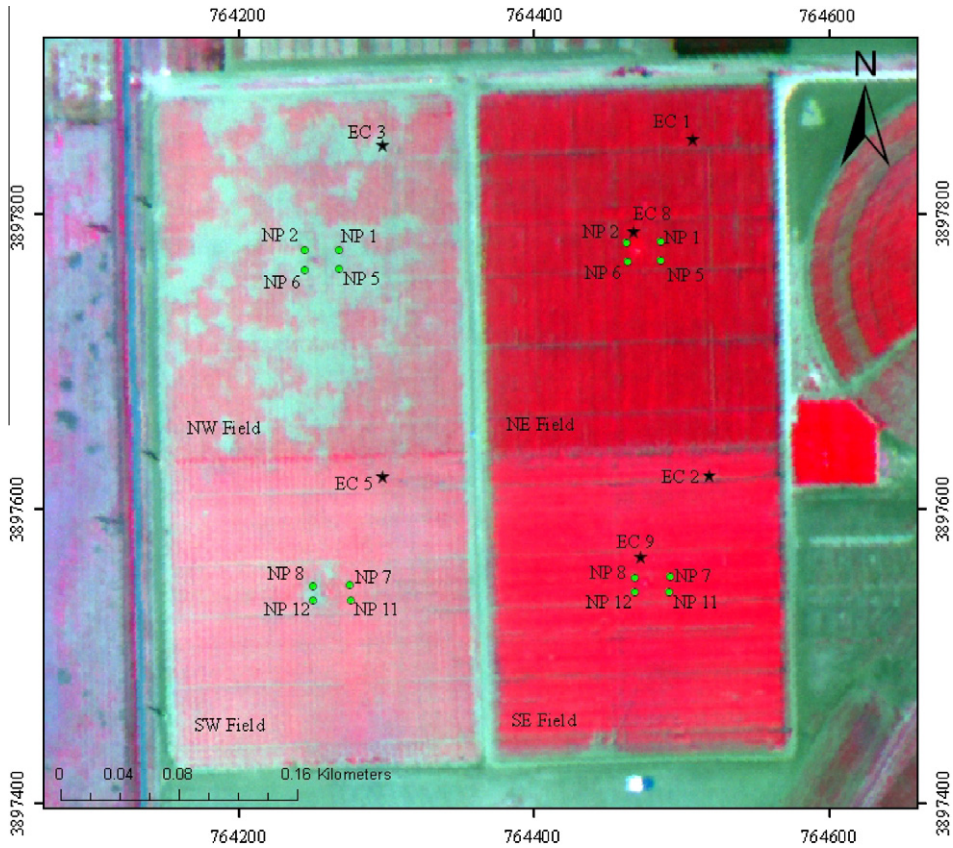

Fig. 1. Description of the study area showing the four cotton fields, the eddy covariance tower locations (stars), neutron probes (green circles), and weather station field (small grass field on the east side) over a 3band multispectral imagery acquired July 28th, 2008.

the soil water content beyond the period of the intensive experiment.

Soil water content in the four cotton fields was measured using the neutron probe method, described in detail in Evett et al. [18]. In Fig. 1, the locations of the neutron probe access tubes and the EC flux towers in the four fields are provided.

2.2. Remote sensing data

High resolution multispectral and thermal infrared images were acquired with the Utah State University airborne digital system throughout the growing season. The system consists of three Kodak Megaplus[1] 4.2i digital cameras with interference filters forming spectral bands in the green (0.545–0.555 μm), red (0.665–0.675 μm) and near infrared (NIR) (0.790–0.810 μm) wavelengths [19,20]. The cameras were mounted through a porthole in a Cessna TP206 aircraft dedicated to remote sensing missions. The cameras were controlled with Epix boards and proprietary software on a desktop computer mounted in the equipment rack. The system's digital cameras were calibrated against a radiance standard in a separate experiment producing calibration curves relating pixel digital number to radiance.

On the day of each image acquisition flight, a standard reflectance panel with known bi-directional properties was set up at the CPRL. An Exotech 4-band radiometer was mounted looking down onto the panel from nadir, measuring incoming irradiance at one-minute intervals of similar spectral bands. This information was used along with the system calibration curves to calculate the reflectance of the pixels in the spectral image mosaics. The individual spectral band images were corrected for lens vignetting effects and radial distortions [20] and registered together into 3-band images. The individual 3-band images were rectified to a National Agriculture Imagery Program (NAIP) 1-meter color digital map base using common control points and stitched together along the flight lines. The flight line strips were calibrated to pixel reflectance using the panel information and then joined together forming a calibrated image mosaic of the entire study area at CPRL. These at-aircraft reflectance images were compared with measurements of surface reflectance collected over cotton and bare soil using ground based multiband radiometers on the day of the over flights, as well as calibration tarps placed on the southern edge of the fields on some flight dates and adjusted linearly to remove atmospheric effects.

The thermal infrared (TIR) images were acquired with an Inframetrics 760 Scanner in the 8–12 μm range. The images were recorded both on S-VHS video tapes and digitally on a laptop computer and later extracted at a 60% overlap along the flight lines for processing. The individual images were geo-rectified to the 3-band calibrated mosaic as a base image map using common control points. The rectified images were stitched along the flight lines and calibrated using the Inframetrics 760 image calibration bar at the bottom of each image which relates digital number to radiometric temperature. The calibrated strips were joined together producing an at-aircraft temperature image mosaic covering the CPRL. The TIR image pixels were then compared with corresponding ground based measurements of surface temperature collected using fixed infrared thermometers and adjusted to these measurements linearly to remove atmospheric effects and correct for surface emissivity.

[1] The use of trade, firm, or corporation names in this article is for the information and convenience of the reader. Such use does not constitute an official endorsement or approval by the United States Department of Agriculture or the Agricultural Research Service of any product or service to the exclusion of others that may be suitable.

Table 1
Airborne image acquisition dates and times.

Date	DOY	Acquisition time (CDT)	Altitude (agl) (m)	MS pixel Res. (m)	TIR pixel Res. (m)	Satellite
26-Jun-08	178	11:40–11:55	2000	1	3	Landsat TM
12-Jul-08	194	11:50–12:35	2000	1	3	Landsat TM
20-Jul-08	202	12:45–12:50	2000	1	3	Aster
28-Jul-08	210	12:30–12:40	2000	1	3	Landsat TM
5-Aug-08	218	12:34–12:50	2000	1	3	Aster
13-Aug-08	226	11:55–12:05	2000	1	3	Landsat TM

The image acquisition dates were selected to coincide with Landsat TM and ASTER overpasses throughout the vegetative growth period of the cotton crop. Information about acquisition dates and image specification such as pixel resolution and acquisition times are listed in Table 1.

3. Methods

3.1. Evapotranspiration models

The remote sensing-based surface energy balance model used in the hybrid approach was the TSEB of Norman et al. [6] with modifications described in Kustas and Norman [21,22] The reflectance-based crop coefficient proposed by Neale et al. [9] was used, applying the SAVI [11] instead of the NDVI as the driving variable [23].

Key formulations of the TSEB model have recently been evaluated over a wide range of canopy cover and environmental conditions [24,7,25]. In this study, the series- formulation of the TSEB model was applied with high resolution aircraft imagery. The main concept behind this formulation is that it separates the surface into soil and canopy components solving the radiation and turbulent energy fluxes for each. Then, at a level above the ground surface called the air-canopy interface, the energy fluxes of each component are combined to represent the total surface energy fluxes. The canopy and soil energy balance is expressed as

$$LE_c = Rn_c - H_c \tag{1a}$$

$$LE_s = Rn_s - G - H_s \tag{1b}$$

where the subscripts c and s refer to the canopy and soil, respectively. The net radiation for the vegetated canopy and soil, Rn_c and Rn_s, were calculated by combining the radiative transfer model of Campbell and Norman [26] into the TSEB model formulation. For a detailed description on how to estimate Rn_c and Rn_s refer to [22].

The model uses the radiometric temperature as the main boundary condition to estimate the energy fluxes. This temperature is partitioned into soil and canopy components as described in Eq. (2).

$$T_R(\phi) \approx [f_c(\phi)T_c^4 + (1 - f_c(\phi))T_s^4]^{1/4} \tag{2}$$

where $f_c(\phi)$ is the fraction of vegetation cover at the radiometer view angle, ϕ, and can be estimated as a function of the leaf area index as $f_c(\phi) = 1 - \exp[-0.5\Omega LAI/\cos(\phi)]$ where Ω represents the clumping factor as described in Kustas and Norman [21] and LAI the leaf area index.

Having the component temperatures, sensible heat flux for the canopy (H_c), soil (H_s), and total (H) are calculated as:

$$H_c = \rho C_P \frac{T_c - T_{ac}}{r_X} \tag{3a}$$

$$H_s = \rho C_P \frac{T_s - T_{ac}}{r_S} \tag{3b}$$

$$H = \rho C_P \frac{T_{ac} - T_a}{r_A} \tag{3c}$$

where ρ is the air density (kg m^{-3}), C_P the specific heat of air ($\sim$ 1013 J kg^{-1} K^{-1}), T_c, T_a, T_s, and T_{ac} the temperatures of the canopy, air, soil, and within canopy air space, respectively (K), r_X the resistance in the boundary layer near the canopy (s m^{-1}), r_S the resistance to heat flux in the boundary layer immediately above the soil surface (s m^{-1}), and r_A the aerodynamic resistance (s m^{-1}). The boundary layer resistance r_X was calculated according to Norman et al. [6] and r_S and r_A were calculated according to Kustas and Norman [21].

For the canopy latent heat flux, a modified form of the Priestley-Taylor equation [27] is used to initially estimate LE_c

$$LE_c = \alpha_{PTC} f_G \frac{\Delta}{\Delta + \gamma} Rn_c \tag{4}$$

Here, α_{PTC} is a variable related to the so-called Priestley-Taylor coefficient, but in this case defined exclusively for the canopy component, as was suggested for row crops by Tanner and Jury [28]. The variable α_{PTC} is normally set to an initial value of $\sim$1.3, except under well watered partial canopy cover conditions in strongly advective environments where a higher value (α_{PTC} $\sim$2) may be more appropriate [21], f_G is the fraction of green vegetation, Δ is the slope of the saturation vapor pressure versus temperature curve, and γ is the psychrometric constant ($\sim$0.058 kPa C^{-1}). Although this study was conducted under strong conditions of advection, the vapor pressure deficits above the irrigated cotton were not significantly large and therefore α_{PTC} was assigned a value of 1.3 [24]. Under stress conditions, the TSEB model iteratively reduces α_{PTC} from its initial value, as described in Kustas and Norman [21] and Li et al. [25].

The latent heat flux from the soil surface is solved as a residual to the soil energy balance equation $LE_s = Rn_s - G - H_s$ with G estimated as a fraction of the net radiation at the soil surface as $G = c_G Rn_s$.

The value of c_G varies with soil type and water content conditions as well as time of day, due to the phase shift between G and Rn_S over a diurnal cycle; however, for the midmorning to midday period, when TIR satellite imagery are typically acquired, the value of c_G can be assumed constant [29].

The hybrid model is programmed within the Spatial Evapo-Transpiration Modeling Interface (SETMI) [30] developed in the ArcGIS environment and includes the TSEB model and the reflectance-based crop coefficient models. Remote sensing inputs can be from either satellite or aircraft platforms. The SETMI model can produce spatial maps of the energy balance fluxes (Rn, G, H and LE) on the date of remote sensing image inputs as well as daily ET maps by extrapolating LE to daily values using either the evaporative fraction or the reference ET fraction [5]. We used the evaporative fraction method in this study as it has been shown to produce more reliable estimates for surfaces with heterogeneous cover under advective conditions [5]. The model also allows the selection of a pixel or group of pixels in the input images corresponding to a location on the surface and estimates the soil water

balance for that location, tracking crop development using the reflectance-based crop coefficient and estimating daily ET over time bridging remote sensing overpass dates. This feature was used to estimate the water balance for pixels surrounding the soil water neutron access tubes.

Spatially-distributed energy fluxes from the TSEB model were compared to measurements from the EC towers by computing the upwind source-area contribution of the turbulent fluxes using a flux footprint model described below. Since the EC systems typically underestimate the turbulent fluxes, H and LE, and because the remote sensing based energy balance model used imposes energy conservation, the closure of the EC data $[(Rn - G) = (LE + H)]$ was forced using the Bowen ratio (H/LE) to partition the missing flux between H and LE [31].

3.2. Footprint model

Generally turbulent flux measurements obtained by Bowen ratio or EC systems are a weighted integral contribution from the upwind source area (SA) or footprint. In this paper we estimated the flux footprint using the model described by Horst and Weil [32,33]. The model provides approximately 90% of the total SA that contributes to the measured fluxes. Flux footprints were utilized to integrate the TSEB model spatial estimates of the four surface energy balance components as well as the daily ET_{TSEB}, which were then compared with the EC measurements for evaluation. In Fig. 2, examples of the estimated flux footprints for two different dates are illustrated. The wind direction was from the north on July 12, so only EC systems 8 and 9 (Fig. 1) were used for comparison on those dates as measurements from the remaining EC flux towers were not representative of the research cotton fields due to their position and sensor orientation. The size and length of the footprints were estimated using measured wind speed, wind direction, the variance of the wind direction distribution, estimated stability variable, the Monin-Obukhov length and aerodynamic roughness length. The apparent differences in shape and size between the footprints we obtained and those estimated by Alfieri et al. [17] for the same EC flux towers were due to two factors: (1) In our analysis the footprints were estimated for the specific hour encompassing the flight overpass time, whereas Alfieri et al. [17] averaged the estimated the footprint for each hour during the day to compute a representative footprint for the day; this included multiple wind directions as winds shifted during the day, resulting in a wider, tear-drop shaped footprint; and (2) Alfieri et al. [17] used the Hsieh et al. [42] footprint model, which is slightly different than the Horst and Weil [32,33] used in this study.

3.3. Soil water balance model

A one dimensional soil water content dynamic model was used to provide estimates of the water content status at multiple layers. The model used was similar to the approach described by Sellers et al. [34]. The soil water content balance on a daily basis for the top layer is modeled using Eq. (5) while all layers below are computed using Eq. (6) as expressed below

$$D_1 \frac{d\theta_1}{dt} = I - E - S_1 - Q_{1,2} \tag{5}$$

$$D_i \frac{d\theta_i}{dt} = Q_{i-1,i} - S_i - Q_{i,i+1} \tag{6}$$

where D is the layer thickness, θ the soil water content, t the time increment, I infiltration rate, E evaporation rate from the soil surface and the upper most layer, i the number of soil layers which varies between 1 and n the total number of soil layers, S_i water uptake from a layer i the root zone, $Q_{i,i+1}$ leakage or soil water flux from layer i to $i + 1$, and Q_n the drainage from the bottom most layer. A detailed description of how to implement and estimate the various components of the model is presented in Geli [15]. In this study, the soil layer depths were selected to match the neutron probe measurement layers and facilitate comparisons.

The water uptake from the different soil layers was estimated from the actual crop ET based on the soil water balance (ET_{WB}) obtained using the crop coefficient as:

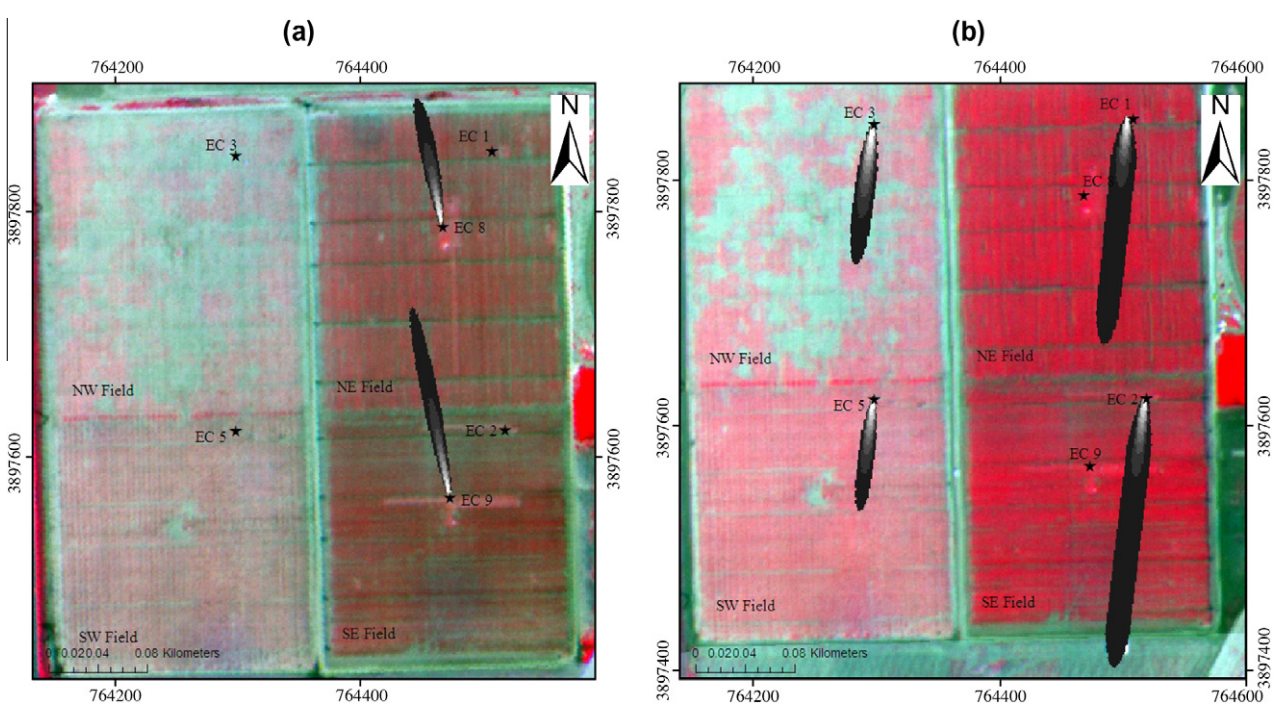

Fig. 2. Upwind flux tower footprints for (a) July 12th (DOY 194) and (b) July 20th (DOY 202) at the time of the aircraft overpass used to weight and integrate the spatially distributed energy balance fluxes.

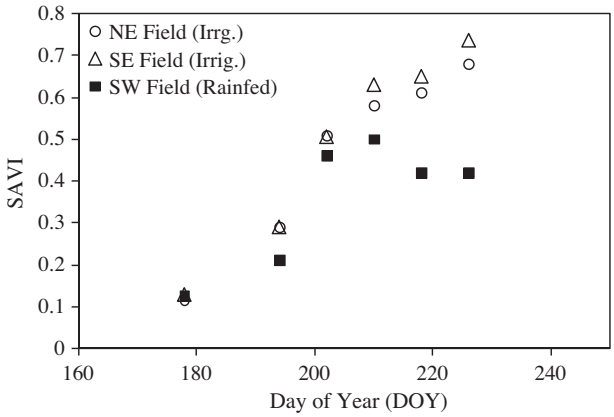

Fig. 3. Progression of the SAVI in three study fields during cotton crop development.

$$ET_{WB} = K_c * ET_0 \tag{7}$$

$$K_c = K_{cb} * K_s + K_e \tag{8}$$

where K_c is the crop coefficient for cotton, K_{cb} the basal crop coefficient updated using the reflectance-based crop coefficient (K_{cbrf}) estimated spatially on each date of airborne image availability, K_s a soil water content deficit coefficient and K_e a soil surface evaporation coefficient applied only on days when the soil surface is wet from an irrigation or rain event [12,13].

3.4. Assimilation of ET_{TSEB} in to ET_{WB}

In the hybrid approach, the analysis starts with the water balance calculations preferably when soil water content is at field capacity in early spring, or after harvest of the previous growing season, incorporating the winter and spring precipitation into the profile. The crop coefficient methodology is then used to initiate the extraction of water by means of actual evapotranspiration. On a specific day that a remote sensing image is available; the K_{cbrf} is then used in the calculation of evapotranspiration instead of the K_{cb}. On this date, two estimates of ET are made, ET_{WB} and ET_{TSEB}. An assumption of the hybrid ET approach is that ET_{TSEB} provides a more reliable estimate than ET_{WB} as it is integrating and representing the soil water availability from estimating soil and canopy temperatures.

The actual ET estimates from the TSEB model (ET_{TSEB}) were assimilated into the soil water balance using the statistical interpolation method [35] as described in Eq. (9).

$$ET^A_{WB} = ET^B_{WB} + W(ET_{TSEB} - ET^B_{WB}) \tag{9}$$

where superscripts A and B refer to after and before assimilation, respectively, and W the weight or Kalman gain of the error for each of the observation points which can be estimated as

$$W = \varepsilon^2/(1+\varepsilon^2) = \sigma^2_B/(\sigma^2_B + \sigma^2_A) \tag{10}$$

where ε^2 is the normalized observation error, σ^2_A and σ^2_B the error variances in ET_{TSM} and ET_{WB} estimates, respectively, with respect to ET measurements. This means that the value of σ^2_B before assimilation is obtained from the error in ET_{WB} with respect to ET_{EC} (ET measured by the EC) and the value of σ^2_A after assimilation resulted from the error in ET_{TSEB} compared to ET_{EC}. In this analysis, the resulting value of W was about 0.86 representing a constant weight applied for the entire period of the study. Detailed description of this methodology can be found in Geli [15] and is also similar to the approach followed by Schuurmans et al. [44]. The assimilated values of ET were used to update soil water content and keep the soil water balance on track with field conditions.

4. Results and discussion

The development of the cotton crop in the study fields can be seen in Fig. 3 where the SAVI at three different access tube locations included in the soil water content modeling has been plotted over time. The SE field had attained greater biomass values than the NE field by Day of Year (DOY) 226 when the last over flight was conducted. This is confirmed by the *LAI* measurements in the same fields described by Evett et al. [18]. Growth rates in the rain fed cotton fields NW and SW were severely hampered, impacted by the low soil water content due to high evaporative demands and lack of precipitation during the early part of the growing season, requiring re-planting and irrigation to promote germination of the seed. Data from the NW field were not used

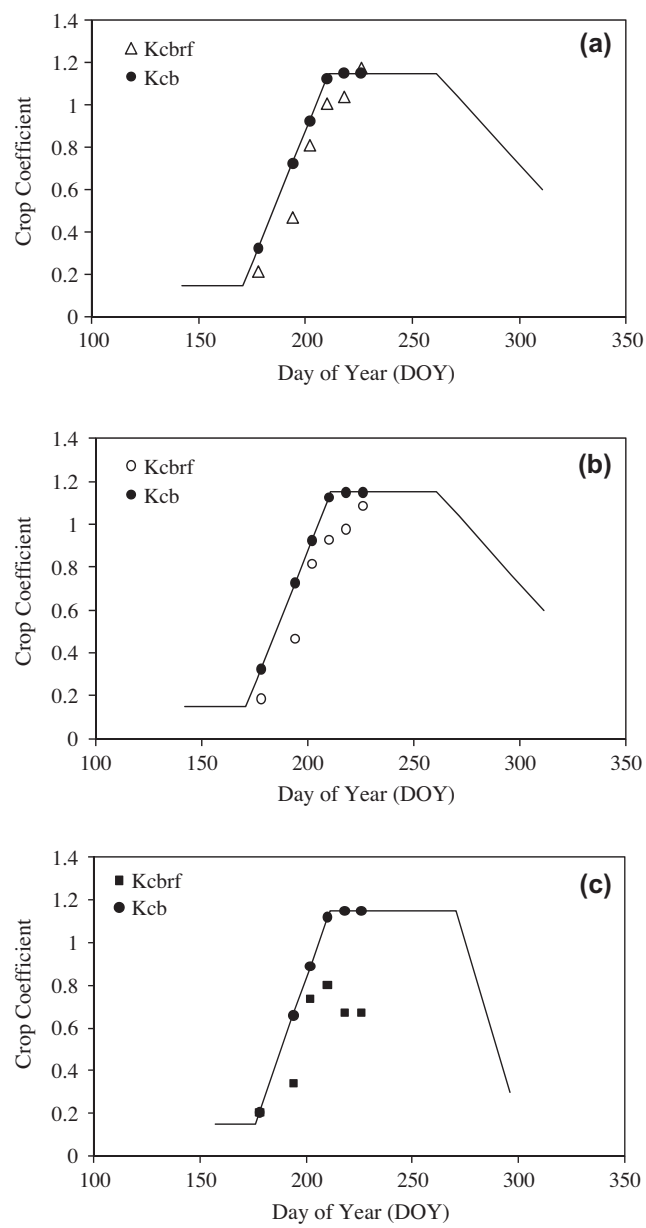

Fig. 4. Basal crop coefficients K_{cb} (FAO56) and remotely sensed K_{cbrf} for the (a) SE and (b) NE irrigated cotton fields and (c) SW dry land cotton field.

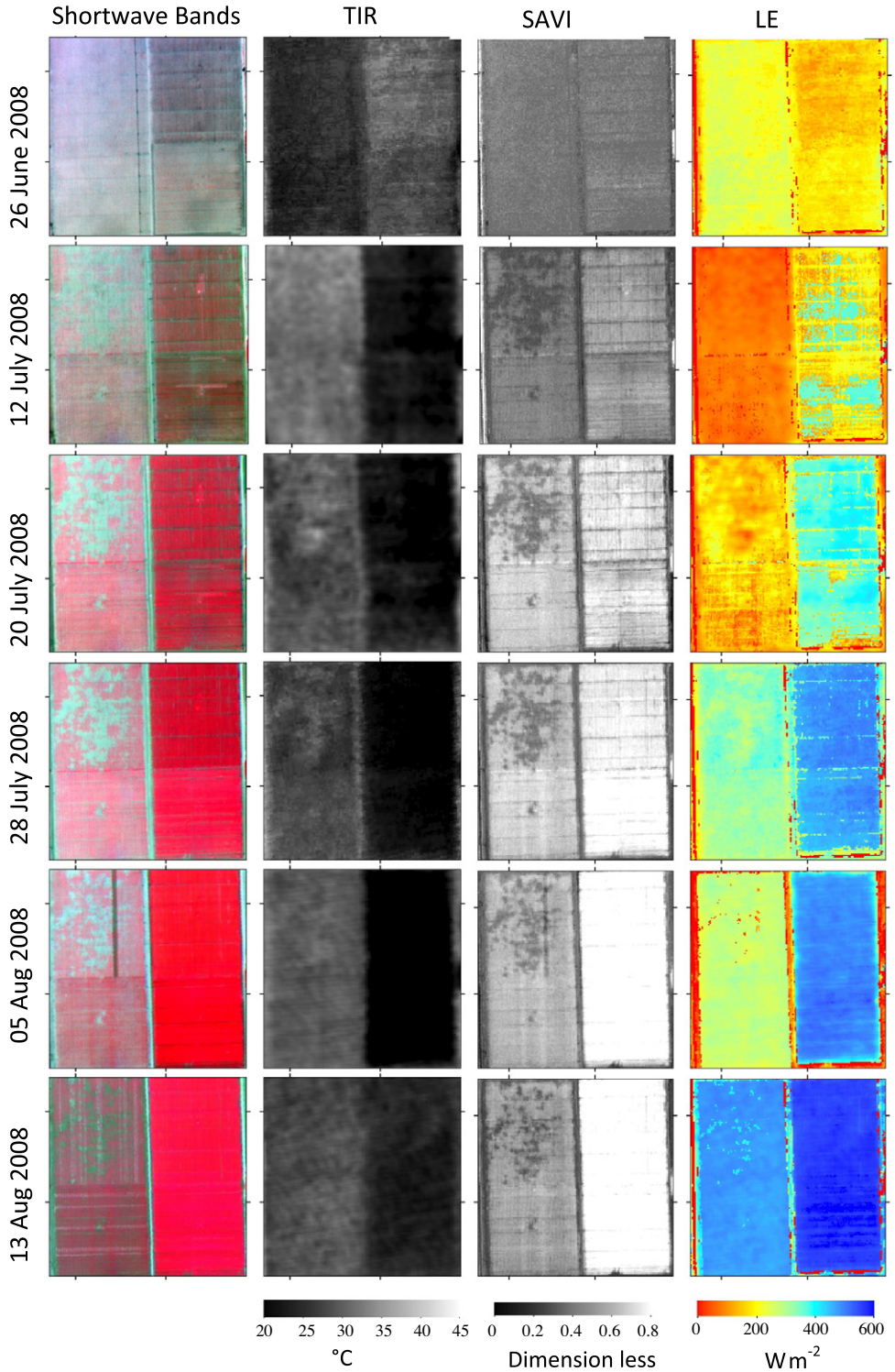

Fig. 5. Image maps showing temporal evolution of 3-band multispectral imagery (Green, Red, NIR shortwave bands), radiometric surface temperature (TIR) and latent heat fluxes (LE) estimated using the TSEB model for the study fields.

for the soil water balance modeling because of poor crop development around the neutron probe access tubes where soil water content was measured (see Fig. 1). As of result of this differential growth in the three fields, the reflectance-based basal crop coefficient did not reach effective full cover for cotton (value of 1.15 as per Allen et al. [13]) in the NE and SW fields by the last flight overpass date, and was almost at that threshold in the SE field (Fig. 4), with some locations (pixels) having reached the effective full cover value, such as the area around the modeled neutron probe location and the locations where the LAI was measured [18].

The spatial patterns of the shortwave bands (false color), thermal-infrared (TIR), SAVI and TSEB-derived LE are illustrated in Fig. 5 for the six dates when airborne imagery was acquired. The spatially distributed four flux components, *Rn*, *G*, *H* and *LE* were integrated over the upwind flux footprint estimated for the EC towers and compared with the measurements from the four cotton

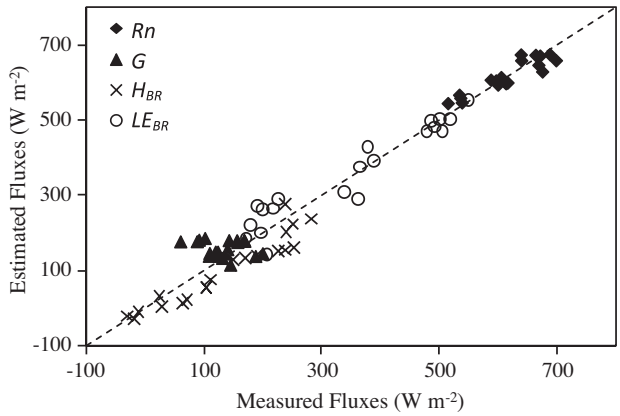

Fig. 6. Estimated surface energy balance components from the TSEB model at the time of aircraft overpass versus observations from the EC towers after forcing closure.

Table 2
Summary of TSEB model performance statistics.

	Rn (W m^{-2})	*G* (W m^{-2})	H_{BR} (W m^{-2})	LE_{BR} (W m^{-2})	ET_{BR} (mm/day)
RMSE	22	50	46	41	0.64
MAE	18	39	40	32	0.53
MBE	1	26	−34	8	0.04

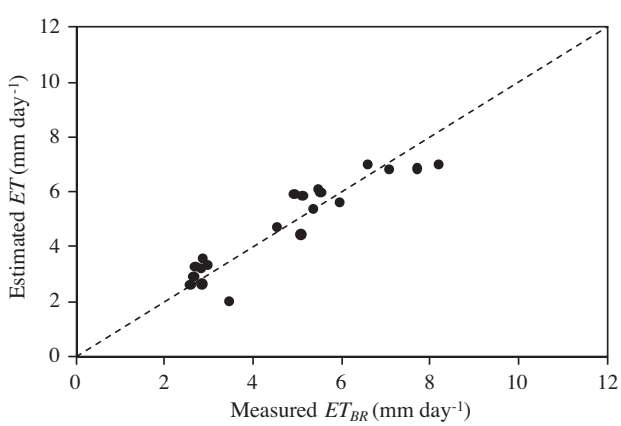

Fig. 7. Estimated and measured daily ET from the EC towers in the four cotton fields on the image acquisition dates shown in Table 1 and Fig. 5.

fields in Fig. 6. Model performance was evaluated using the root mean square error (RMSE), the mean absolute error (MAE), and the mean bias error (MBE) and presented in Table 2. Results indicate that the TSEB model reproduces fluxes for both irrigated and rain fed cotton fields comparable with other studies that applied the TSEB model with ground-based and/or satellite remote sensing data collected during BEAREX08 [36–38]. However, in using the high resolution airborne imagery, this is the only study of this experiment that was able to compute a detailed upwind flux footprint contribution of model output to compare with the eddy covariance measurements. The instantaneous LE fluxes were extrapolated to daily ET values using the reference ET fraction and compared to daily ET measured with the EC systems adjusted for closure using the Bowen ratio approach (Fig. 7). The performance statistics are also shown in Table 2 and indicate a relatively small bias and MAE value.

The hybrid approach was applied to pixels surrounding 3 representative access tubes, one in each field (NE, SE and SW)

Table 3
Performance/difference statistics for estimated profile of soil water content using the water balance model without and with assimilation of ET estimated with the TSEB model.

Fields and layers	Without assimilation		With assimilation	
	RMSE (mm)	MBE (mm)	RMSE (mm)	MBE (mm)
NE field				
Layer depth (cm)				
0–20	10.1	−5.9	10.0	−3.4
20–40	10.2	−2.8	6.8	0.3
40–60	5.5	2.2	5.0	3.6
60–80	5.0	1.0	3.2	2.6
80–100	2.4	−0.2	2.2	0.1
100–120	5.1	−5.0	5.1	−4.9
All layers	19.6	−10.7	10.0	−1.7
SE field				
Layer depth (cm)	10.9	−7.3		
0–20	10.5	−6.4	9.6	−5.7
20–40	7.5	−1.8	8.0	−4.9
40–60	7.5	2.9	5.9	−0.7
60–80	5.3	4.4	7.7	4.2
80–100	3.0	1.7	5.8	5.4
100–120	3.1	2.9	3.0	2.2
All layers	23.9	−6.5	17.7	0.5
SW field				
Layer depth (cm)				
0–20	7.5	1.7	6.8	2.3
20–40	8.3	−5.1	7.5	−4.4
40–60	4.3	0.0	3.9	0.6
60–80	9.9	7.0	10.6	9.8
80–100	7.4	5.5	6.5	4.3
100-120	6.6	−6.6	6.6	−6.6
All layers	20.4	2.6	17.6	6.2
All fields	21.5	−6.8	14.9	0.6

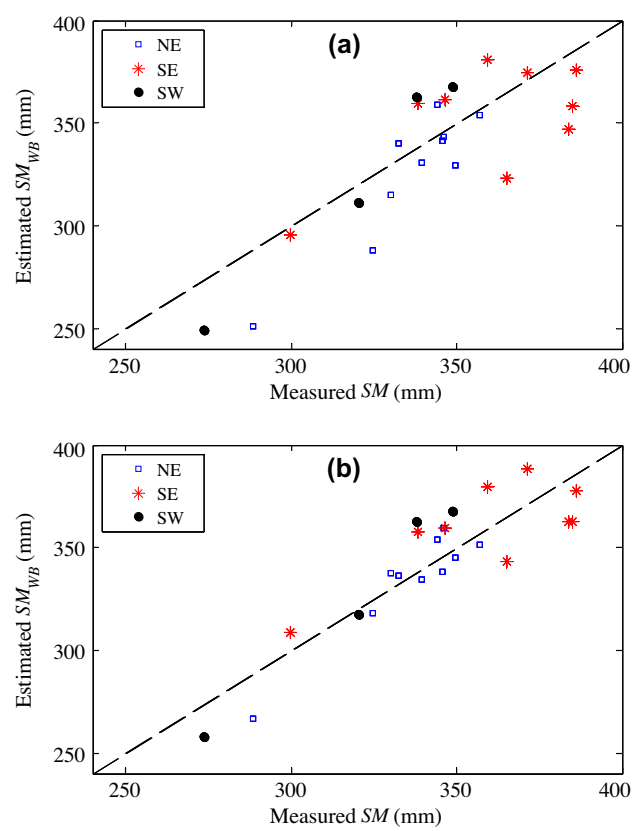

Fig. 8. Modeled total soil water content in the root zone (1.2 m) (a) before and (b) after assimilation for all fields.

and captured a range of LAI and biomass and growth patterns. The soil water balance was conducted at each location first without assimilation using the K_{cbrf} approach. As shown in Fig. 4, the values of the K_{cbrf} throughout growing season were lower than those tabulated by Allen et al [13]. This is an advantage of the K_{cbrf} method which tracks the actual growth conditions in the field. These differences in crop coefficients will impact the modeled soil water content in the root zone and thus the estimated ET. In Table 3 the estimated soil water content values with and without assimilation of ET are compared with the measurements for the different soil layers modeled. Note that estimates of soil water content were computed for 7 layers, each 20 cm in thickness, centered at 0.1, 0.3, 0.5, 0.7, 0.9, and 1.10 meters. When assimilating ET, the results obtained from the TSEB model applied to the airborne imagery (ET_{TSEB}) were used and the soil water balance recalculated resulting in an improved estimation of the soil water content (see Table 3) with smaller difference statistics by layer modeled and for the total root zone profile (Fig. 8). Before assimilation, the RMSE values for the total root zone profile were 19.6, 23.9, and 21.5 mm for the NE, SE, and SW fields, respectively. After assimilation the RMSE values were reduced to 10.0, 17.7, and 17.6 mm for the same fields. Likewise, before assimilation the soil moisture for the total profile was underestimated for the three fields (see MBE values in Table 3), while after assimilation the MBE was greatly reduced to less than one millimeter for the SE and SW fields.

Overall, the soil water content estimates look reasonable for both irrigated and rain fed fields. This is an important point to consider, since modeling soil water content in irrigated areas is generally more accurate than in rain fed agriculture, due to the re-setting of the soil profile to field capacity after each irrigation event. In rain fed agricultural areas there is greater vertical variability of soil water content affecting plant uptake [43] along with greater spatial variability due to non-uniform precipitation input across a landscape. The study by Geli [15] conducted over rain fed fields in central Iowa under minimal advective conditions, obtained similar results to the current study for the top-30 cm of the soil profile, but over spatial scales of about 10 by 30 km.

However it is important to note that there was a general tendency for larger discrepancies between modeled and observed soil water content for the top two soil layers. This was due in part to the greater spatial and temporal variability in the soil water content observed near the surface during this experiment [39]. It is also possible that the root distribution/extraction model we used for cotton might require further refinement to be applicable to the particular soil type and crop variety used in this study.

5. Conclusions

The TSEB model as programmed in the SETMI environment and using high resolution airborne imagery as input provided reliable instantaneous and daily *LE*, (Table 2) The estimated soil water content profiles from a water balance model were compared to several neutron probe access tube locations using ET estimates from the crop coefficient method and also by assimilating the TSEB model computed ET. The differences between the modeled and observed soil water content values using the neutron probe technique indicated that the assimilation of ET values from the TSEB model significantly improved the agreement. This suggests that assimilation of robust actual ET estimates from a thermal-based surface energy balance model can significantly improve a water balance model output of profile soil water content as suggested earlier by Crow et al. [40]. In addition, there are other soil water content metrics from the TSEB model that have been assimilated into water balance models and shown to significantly improve soil water content profile estimates [41]. There was a tendency for larger discrepancies between modeled and observed soil water content estimates in the top layers of the root zone. This was due in part to the inherent increased variability in near surface water content, but also differences could be decreased by using an improved, more robust root distribution and extraction model for the cotton variety. This will be evaluated in a future study with these data.

This paper represents a progression of research effort towards providing improved spatial-temporal estimates of ET and soil water content in the root zone of agricultural crops through a hybrid ET approach tested over both irrigated and rain fed agricultural fields. Plans are underway to evaluate this hybrid ET model over irrigated agricultural areas within scales of 8 and 12 digits HUC (hydrological Unit Codes) of the U. S. Geological Survey.

Acknowledgements

This research was funded in part by the USDA-ARS Conservation & Production Research Laboratory, Bushland, TX, the USDA-ARS Hydrology and Remote Sensing Laboratory, Beltsville, MD, and the Remote Sensing Services Laboratory, Dept. of Civil and Environmental Engineering, Utah State University. Hatim Geli was supported by the Utah Water Research Laboratory and Christopher Neale by the Utah Agricultural Experiment Station.

References

[1] Anderson MC, Kustas WP, Norman JM, Hain CR, Mecikalski JR, Schultz L, et al. Mapping daily evapotranspiration at field to continental scales using geostationary and polar orbiting satellite imagery. Hydrol Earth Syst Sci 2011;15:223–39.
[2] Bastiaansen WGM, Menenti M, Feddes RA, Holtslag AAM. A remote sensing surface energy balance algorithm for land (SEBAL): 1. Formulation. J Hydrol 1998;212:198–212.
[3] Allen RG, Tasumi M, Trezza R. Satellite-based energy balance for mapping evapotranspiration with internalized calibration (METRIC)-Model. J Irrigation Drainage Syst 2007;133:380–94.
[4] Colaizzi PD, Evett SR, Howell TA, Tolk JA. Comparison of five models to scale daily evapotranspiration from one-time-of day measurements. Trans ASABE 2006;49:409–1417.
[5] Chavez JL, Neale CMU, Prueger JH, Kustas WP. Daily evapotranspiration estimates from extrapolating instantaneous airborne remote sensing ET values. Irrigation Sci 2008;27:67–81.
[6] Norman JM, Kustas WP, Humes KS. A two-source approach for estimating soil and vegetation energy fluxes in observations of directional radiometric surface temperature. Agric Forest Meteorol 1995;77:263–93.
[7] Kustas WP, Anderson MC. Advances in thermal infrared remote sensing for land surface modeling. Agric Forest Meteorol 2009;149:2071–81.
[8] Bausch WC, Neale CMU. Crop coefficients derived from reflected canopy radiation: a concept. Trans ASAE 1987;30:703–9.
[9] Neale CMU, Bausch W, Heermann D. Development of reflectance based crop coefficients for corn. Trans ASAE 1989;32:1891–9.
[10] Rouse JW, Haas RH, Schell JA, Deering DW. Monitoring vegetation systems in the great plains with ERTS. Third ERTS symposium. NASA SP-351 1973;I:309–17.
[11] Huete AR. A soil adjusted vegetation index (SAVI). Rem Sens Environ 1988;25:295–309.
[12] Wright JL. New evapotranspiration crop coefficients. J Irrg Drain Div ASCE 1982;108:57–74.
[13] Allen R, Pereira L, Raes D, Smith M. Crop evapotranspiration (guidelines for computing crop water requirements). FAO irrigation and drainage paper no. 56. FAO, Rome, Italy; 1998.
[14] Neale CMU, Vinukollu RK, Ramsey RD. A hybrid surface energy balance approach for the estimation of evapotranspiration in agricultural areas. In: D'Urso G, Osann Jochum MA, Moreno J, editors. Earth observation for vegetation monitoring and water management, Naples, Italy, 10–11 November 2005. AIP conference proceedings, vol. 852; 2005. ISBN: 9780735 403468.
[15] Geli HME. Modeling surface energy fluxes of agricultural and riparian vegetation using remote sensing. Ph.D. dissertation. Department of Civil and Environmental Engineering, Utah State University; 2012.
[16] Evett SR, Kustas WP, Gowda PH, Howell TA. Overview of the Bushland Evapotranspiration (ET) and Agricultural Remote sensing EXperiment 2008 (BEAREX08). A remote sensing field experiment evaluating model and measurement techniques quantifying ET at the canopy, sub-field, multi-field and at regional scales, Adv Water Resour 2012;50:4–19.
[17] Alfieri JG, Kustas WP, Prueger JH, Hipps LE, Evett SR, Basara JB, et al. On the discrepancy between eddy covariance and lysimetry-based turbulent flux

measurements under strongly advective conditions Adv Water. Resour 2012;50:62–78.
[18] Evett SR, Schwartz RC, Howell TA, Baumhardt RL, Copeland KS. Can weighing lysimeter ET represent surrounding field ET well enough to test flux station measurements of daily and sub-daily ET?. Adv Water Resour 2012;50:79–90.
[19] Cai B, Neale CMU. A method for constructing three dimensional models from airborne imagery. 17th Biennial workshop on color photography and videography in resource assessment. May 5–7, 1999. Held at Peppermill Hotel and Casino. Reno – Nevada. Cosponsored by the American Society for Photogrammetry and Remote Sensing and Department of Environmental and Resource Science, University of Nevada; 1999.
[20] Neale CMU, Crowther B. An airborne multispectral video/radiometer remote sensing system: development and calibration. Remote Sens Environ 1994;49:187–94.
[21] Kustas WP, Norman JM. Evaluation of soil and vegetation heat flux predictions using a simple two-source model with radiometric temperatures for partial canopy cover. Agric Forest Meteorol 1999;94:13–29.
[22] Kustas WP, Norman JM. A two-source energy balance approach using directional radiometric temperature observations for sparse canopy covered surface. Agronomy J 2000;92:847–54.
[23] Neale CMU, Ahmed RH, Moran MS, Pinter Jr PJ, Qi J, Clarke TR. Estimating cotton seasonal evapotranspiration using canopy reflectance. Proceedings of the international conference on evapotranspiration and irrigation scheduling, November 3–6, San Antonio, Texas; 1996.
[24] Agam N, Kustas WP, Anderson MC, Norman JM, Colaizzi PD, Howell TA, et al. Application of the Priestley–Taylor approach in a two-source energy balance model. J Hydrometeorol 2010;11:185–98.
[25] Li F, Kustas WP, Prueger JH, Neale CMU, Jackson TJ. Utility of remote sensing based two-source energy balance model under low and high vegetation cover conditions. J Hydrometeorol 2005;6:878–91.
[26] Campbell GS, Norman JM. An introduction to environmental biophysics. 2nd ed. Springer; 1998.
[27] Priestley CHB, Taylor RJ. On the assessment of surface heat flux and evaporation using large-scale parameters. Mon Weather Rev 1972;100:81–92.
[28] Tanner CB, Jury WA. Estimating evaporation and transpiration from a row crop during incomplete cover. Agronomy J 1976;68:239–43.
[29] Santanello JA, Friedl MA. Diurnal variation in soil heat flux and net radiation. J Appl Meteorol 2003;42:851–62.
[30] Geli HME, Neale CMU. Spatial EvpoTranspiration Modeling Interface (SETMI), remote sensing and hydrology 2010. Wyoming, USA: Jackson Hole; 2010.
[31] Twine TE, Wesely. Correcting eddy-covariance flux underestimates over a grassland. Agric Forest Meteorol 2000;103:279–300.
[32] Horst TW, Weil JC. Footprint estimation for scalar flux measurements in the atmospheric surface layer. Boundary-Layer Meteorol 1992;59: 279–96.
[33] Horst TW, Weil JC. How far is far enough? The fetch requirements for micrometeorological measurement of surface fluxes. J Atmos Oceanic Technol 1994;11:1018–25.
[34] Sellers PJ, Mintz Y, Sud YC, Dalcher A. A simple biosphere model (SIB) for use within general circulation models. J Atmos Sci 1986;43:505–31.
[35] Daley R. Atmospheric data assimilation. Cambridge University Press; 1991.
[36] Anderson MC, Kustas WP, Alfieri JG, Gao F, Hain CR, Evett SR, et al. Mapping daily evapotranspiration at landsat spatial scales during the BEAREX'08 field campaign. Adv Water Resour 2012;50:162–77.
[37] Colaizzi PD, Kustas WP, Anderson MC, Gowda PH, O'Shaughnessy SA, Howell TA, et al. Two-source model estimates of evapotranspiration using component and composite surface temperatures. Adv Water Resour 2012;50:134–51.
[38] Kustas WP, Alfieri JG, Anderson MC, Colaizzi PD, Prueger JH, Evett SR, et al. Evaluating the two-source energy balance model using local thermal and surface flux observations in a strongly advective irrigated agricultural area. Adv Water Resour 2012;50:120–33.
[39] Cosh MH, Evett SR, McKee LG. Surface soil water content spatial organization within irrigated and non-irrigated agricultural fields. Adv Water Resour 2012;50:55–61.
[40] Crow WT, Li F, Kustas WP. Intercomparison of spatially distributed models for predicting surface energy flux patterns during SMACEX. J Hydromet 2005;6:941–53.
[41] Crow WT, Kustas WP, Prueger JH. Monitoring root zone soil though the assimilation of a thermal remote sensing based soil proxy into a water balance model. Remote Sens Environ 2008;112:1268–81.
[42] Hsieh C-I, Katul G, Chi T-W. An approximate analysis model for footprint estimation of scalar fluxes in the thermally stratified atmospheric flows. Adv Water Res 2000:765–72.
[43] Guswa AJ, Celia MA, Rodriguez-Iturbe I. Models of soilmoisture dynamics in ecohydrology: a comparative study. Water Resour Res 2002;38(9).
[44] Schuurmans JM, Troch PA, Veldhuizen AA, Bastiaanssen WGM, Bierkens MFP. Assimilation of remotely sensed latent heat flux in a distributed hydrological model. Adv Water Resour 2003;26:151–9.